Atmos. Chem. Phys. Discuss., https://doi.org/10.5194/acp-2019-313
Manuscript under review for journal Atmos. Chem. Phys.
Discussion started: 13 May 2019

Atmospheric Chemistry and Physics Discussions

Effects of stabilized Criegee Intermediates (sCI) on the sulfate formation: A sensitivity analysis during summertime in Beijing-Tianjin-Hebei (BTH), China

Lang Liu[1,3,4], Naifang Bei[2], Jiarui Wu[1,3], Suixin Liu[1,3], Jiamao Zhou[1,3], Xia Li[1,3], Qingchuan Yang[1], Tian Feng[1], Junji Cao[1,3], Xuexi Tie[1], Guohui Li[1,3*]

[1]Key Lab of Aerosol Chemistry and Physics, SKLLQG, Institute of Earth Environment, Chinese Academy of Sciences, Xi'an, 710061, China
[2]School of Human Settlements and Civil Engineering, Xi'an Jiaotong University, Xi'an, Shaanxi, 710049, China
[3]CAS Center for Excellence in Quaternary Science and Global Change, Xi'an, 710061, China
[4]University of Chinese Academy of Sciences, Beijing, 100049, China

Correspondence to: Guohui Li (ligh@ieecas.cn)

Abstract: Sulfate aerosols exert profound impacts on climate, ecosystem, visibility, and public health, but the sulfate formation pathway remains elusive. In the present study, a source-oriented WRF-Chem model is applied to simulate a persistent air pollution episode from 04 to 15 July 2015 in Beijing-Tianjin-Hebei (BTH), China to study contributions of four pathways to the sulfate formation. When comparing simulations to measurements in BTH, the index of agreement (IOA) of meteorological parameters, air pollutants and aerosol species generally exceeds 0.6. On average in BTH, the heterogeneous reaction of SO_2 involving aerosol water and the SO_2 oxidation by OH constitutes the two most important sulfate sources, with a contribution of about 35~38% and 33~36% respectively. The primary emission accounts for around 22~24% of sulfate concentrations due to high SO_2 emissions. The SO_2 oxidation by stabilized Criegee Intermediates (sCI) also plays an appreciable role in the sulfate formation, with a contribution of around 9% when an upper limit of the reaction rate constant of sCI with SO_2 (κ_{sCI+SO_2}=3.9×10^{-11} cm^3 s^{-1}) and a lower limit of the reaction rate constant of sCI with H_2O (κ_{sCI+H_2O}=1.97×10^{-18} cm^3 s^{-1}) are used. Sensitivity studies reveal that there still exist large uncertainties in the sulfate contribution of the SO_2 oxidation by sCI. The sulfate contribution of the reaction is decreased to less than 3% when κ_{SCI+SO_2} is decreased to 6.0×10^{-13} cm^3 s^{-1}. Furthermore, when κ_{sCI+H_2O} is increased to 2.38×10^{-15} cm^3 s^{-1} based on the reported ratio of κ_{SCI+H_2O} to κ_{SCI+SO_2} (6.1×10^{-5}), the sulfate contribution becomes insignificant, less than 2%. Further studies need to be conducted to better determine κ_{sCI+SO_2} and κ_{sCI+H_2O} to evaluate effects of the sCI chemistry on the sulfate formation.

Atmos. Chem. Phys. Discuss., https://doi.org/10.5194/acp-2019-313
Manuscript under review for journal Atmos. Chem. Phys.
Discussion started: 13 May 2019

1 Introduction

As a major component of fine particulate matters ($PM_{2.5}$) in the atmosphere, sulfate aerosols not only directly and indirectly influence regional and global climate, also impair ecosystem, visibility and potentially public health (e.g., Wang and Hao, 2012; Guo et al., 2014; Gao et al., 2016; Tao et al., 2017). Sulfate aerosols are primarily formed through homogeneous and heterogeneous oxidations of sulfur dioxide (SO_2) emitted from anthropogenic and natural sources (Seinfeld and Pandis, 2006). The sulfate formation pathway via the SO_2 oxidation includes aqueous reactions in cloud or fog droplets, heterogeneous reactions associated with aerosol water, and gas-phase reactions with hydroxyl radicals (OH) and stabilized Criegee Intermediates (sCI) (Seinfeld and Pandis, 2006; Wang et al., 2016; Li et al., 2017). Recent studies have revealed that the SO_2 oxidation by sCI could constitute an important sulfate source in the atmosphere (Welz et al., 2012; Mauldin et al., 2012; Boy et al., 2013; Pierce et al., 2013; Percival et al., 2013).

Carbonyl oxide intermediates formed in the ozonolysis reaction of alkenes, often known as sCI, are proposed to be important radicals in the atmosphere. In the gas phase, sCI can act as an additional atmospheric oxidant. Laboratory studies in the 1970s have shown that the SO_2 oxidation is enhanced in the presence of alkenes and ozone, providing the first evidence that sCI could react with SO_2 (Cox and Penkett, 1971). In the 2010s, Welz et al. (2012) have used photoionization mass spectrometry to make the first direct measurement of individual sCI isomers. They have found that the reaction rate of the simplest sCI, H_2COO, with SO_2 is faster than expected by up to three orders of magnitude, whereas the removal of sCI by water vapor is comparatively slow. The result has also indicated that the sCI chemistry potentially contributes substantially to the SO_2 oxidation, and exerts profound effects on the sulfate formation. Basing on the laboratory experiments and theoretical considerations, Mauldin et al. (2012) have reported the reaction rate of the sCI originated from the ozonolysis reaction of

α-pinene and limonene with SO_2 under boundary layer atmospheric conditions. The new reaction rates are slower than those found in Welz et al. (2012), but still about one order of magnitude faster than previously used (Jenkin et al., 1997).

Further studies have been conducted to evaluate contributions of the SO_2 oxidation by sCI to the sulfate in the atmosphere, based on the results of Welz et al. (2012) and Mauldin et al. (2012). Boy et al. (2013) have examined effects of the increased reaction rate of sCI with SO_2 on the atmospheric sulfuric acid (H_2SO_4) concentration at two stations, showing that the reaction contributes as much as 33-46% of H_2SO_4 concentrations at the ground level. Using the results of Welz et al. (2012), Sarwar et al. (2013) have shown that the SO_2 oxidation by sCI does not substantially influence sulfate concentrations in the USA due to the competing reaction of sCI with water vapor. However, when using the high reaction rate constant of sCI with SO_2 (κ_{sCI+SO_2}) and the low reaction rate constant of sCI with H_2O (κ_{sCI+H_2O}) simultaneously, the SO_2 oxidation by sCI considerably enhances the sulfate formation (Sarwar et al., 2014). Li et al. (2013) have demonstrated that the SO_2 oxidation by sCI contributes about 18% of the sulfate concentration during summertime in the eastern USA, when using the κ_{sCI+SO_2} reported by Welz et al. (2012). Pierce et al. (2013) have used the same κ_{sCI+SO_2} in simulations of the GEOS-CHEM model, showing that the reaction increases the H_2SO_4 production globally by 4%, and the induced H_2SO_4 enhancement is almost entirely distributed over the forested continental regions with large fluxes of biogenic alkene emissions.

With rapid industrialization and urbanization, heavy air pollution with high levels of $PM_{2.5}$ and/or ozone (O_3) frequently occurs in Beijing-Tianjin-Hebei (BTH), and sulfate aerosols have become a main component of $PM_{2.5}$ (e.g., Zhang et al., 2012; Zhao et al., 2013; Sun et al., 2015; Li et al., 2017; Wu et al., 2017). Considering the high alkenes emissions and increasing trend of O_3 concentrations during summertime in BTH, it is imperative to assess

effects of the sCI chemistry on the sulfate formation. In the present study, a source-oriented WRF-Chem model has been developed and applied to study the contribution of different pathways to the sulfate formation in BTH during the summer of 2015. The model configuration and methodology are described in Section 2. Results and discussions are presented in Section 3. The conclusions and summaries are drawn in Section 4.

2 Model and methodology

2.1 WRF-CHEM model and configuration

A specific version of the WRF-Chem model (Grell et al., 2005) developed by Li et al. (2010; 2011a; 2011b; 2012) at the Molina Center for Energy and the Environment is used in the present study. Detailed model description can be found in previous studies (Li et al., 2018; Wu et al., 2017; Feng et al., 2016; Xing et al., 2019). Briefly, the model includes a new flexible gas-phase chemical module and the Community Multi-scale Air Quality (CMAQ) aerosol module developed by the US EPA (Binkowski and Roselle, 2003). The wet deposition uses the method in the CMAQ module and the dry deposition of chemical species is parameterized following Wesely (1989). The photolysis rates are calculated using the Fast Tropospheric Ultraviolet and Visible Radiation Model (FTUV; Li et al., 2005; Tie et al., 2003), with the aerosol and cloud effects on the photochemistry (Li et al., 2011a). The ISORROPIA Version 1.7 is applied to calculate the inorganic components (Nenes et al., 1998). The secondary organic aerosol (SOA) is simulated using a non-traditional module, including the volatility basis-set (VBS) modeling approach and SOA contributions from glyoxal and methylglyoxal.

Traditionally, the brute force method (BFM) is generally used to quantify the formation pathway of particulate matters and chemical compounds in modeling studies (Dunker et al., 1996). The BFM method evaluates the importance of the certain formation pathway through

including and excluding the pathway in simulations, but it lacks consideration of interactions of the complicated physical and chemical processes in the atmosphere (Zhang and Ying, 2011). The source-oriented method introduces additional chemical species to represent formations from different pathways, providing direct and quantitative determination of contributions of different pathways (Ying and Krishnan, 2010). The coupled source-oriented method air quality models have been widely used to study source apportionment of particulate matters and chemical compounds. Detailed description about the method can be found in previous studies (Ying and Kleeman, 2006; Ying and Krishnan, 2010; Zhang and Ying, 2011). In the present study, four reactive tagged species are introduced to track the sulfate formation pathways.

A persistent air pollution episode with high levels of O_3 and $PM_{2.5}$ from 04 to 15 July 2015 in BTH is simulated in association with the observation of air pollutants and secondary aerosols. Detailed information about the episode can be found in Wu et al. (2017). Figure 1 shows the WRF-Chem model simulation domain and Table 1 presents the model configuration.

2.2 Simulations for the sulfate aerosols

Four sulfate formation pathways are considered in the WRF-Chem model, including (1) the heterogeneous reaction of SO_2 involving aerosol water (hereafter referred to as HR_SO_2), (2) the SO_2 oxidation by OH (hereafter referred to as OH_SO_2), (3) the primary emission, and (4) the SO_2 oxidation by sCI (hereafter referred to as sCI_SO_2). The sulfate formed in the four pathways is tagged and traced in the model to study their contributions to the sulfate formation. It is worth noting that the WRF-Chem model cannot well resolve clouds formed in the planetary boundary layer (PBL), so the aqueous SO_2 oxidation in cloud or fog droplets is not considered in the study, which might cause the sulfate underestimation. The HR_SO_2 is parameterized as a first-order irreversible uptake of SO_2 by aerosol water, with a reactive

uptake coefficient of 0.5×10^{-4}, assuming that alkalinity is sufficient to maintain the high iron-catalyzed reaction rate in BTH (Li et al., 2017).

Effects of the sCI chemistry on the sulfate formation depend on κ_{sCI+SO_2} and κ_{sCI+H_2O}, as well as the sCI precursor concentration. In the study, sCI are assumed to yield from the ozonolysis reaction of five alkenes based on the SAPRC99 mechanism, including ethene (ETHE), terminal olefin (OLE1), internal olefin (OLE2), isoprene (ISOP), and monoterpenes (TERP). Detailed information about the sCI chemistry associated with the sulfate formation can be found in Table 2.

CH_2OO (sCI_1) is used to represent sCI produced from the ozonolysis reaction of ETHE and OLE1 and the sCI yield of the two reactions are described in Sarwar et al. (2013). CH_3CHOO (sCI_2) is formed from the ozonolysis reaction of OLE2, and proposed to have two isomers: *syn*-CH_3CHOO and *ant*-CH_3CHOO (Anglada et al., 2011). The reported reaction rate constants of *syn*-CH_3CHOO and *ant*-CH_3CHOO with H_2O are 3.23×10^{-18} and 3.23×10^{-13} $cm^3\ s^{-1}$, respectively. We use *syn*-CH_3CHOO (sCI_2) to represent the sCI from the ozonolysis reaction of OLE2 to minimize the removal of sCI by water vapor and maximize sulfate production following Ying et al. (2014). sCI_3 is used to represent sCI from the ozonolysis reaction of isoprene and monoterpenes, and the detailed chemistry of sCI_3 is descripted in Sarwar et al. (2013, 2014).

In the base case (hereafter referred to as B-case) simulation used to compare with observations in BTH, we use a single κ_{sCI+SO_2} reported by Welz et al. (2012) for reactions of SO_2 with $sCI_{1,2,3}$. For removal of $sCI_{1,2,3}$ by water vapor, we employ the κ_{sCI+H_2O} suggested by Ying et al. (2014). While not important, the reaction of $sCI_{1,2,3}$ with NO_2 is also implemented in the model, and the rate constant is taken from Welz et al. (2012).

2.3 Observations

Simulations are compared to available meteorological and air pollutants observations to validate the model performance. The meteorological parameters including surface temperature (TSFC), relative humidity (RH), wind speed and direction with a 3-hour interval are obtained from the website http://www.meteomanz.com. The hourly measurements of $PM_{2.5}$, O_3, SO_2, and NO_2 used in this study are downloaded from the website http://www.aqistudy.cn. The submicron sulfate, nitrate, ammonium, and organic particulate matters are observed by the Aerodyne Aerosol Chemical Speciation Monitor (ACSM) at the National Center for Nanoscience and Technology (NCNST), Chinese Academy of Sciences, Beijing (116.39°E, 39.99°N). Detailed description about the methods to obtain the primary organic aerosol (POA) and secondary organic aerosol (SOA) mass concentration from the results of ACSM are given in Wu et al. (2017). Figure 1 shows the locations of the ambient air quality monitoring sites and the NCNST observation site.

2.4 Statistical methods for model evaluation

In this study, the mean bias (MB), root mean square error (RMSE) and the index of agreement (IOA) are used to evaluate the model performance:

$$MB = \frac{1}{N}\sum_{i=1}^{N}(P_i - O_i) \quad (1)$$

$$RMSE = \left[\frac{1}{N}\sum_{i=1}^{N}(P_i - O_i)^2\right]^{\frac{1}{2}} \quad (2)$$

$$IOA = 1 - \frac{\sum_{i=1}^{N}(P_i - O_i)^2}{\sum_{i=1}^{N}(|P_i - \bar{O}| + |O_i - \bar{O}|)^2} \quad (3)$$

Where P_i and O_i are the simulated and observed variables, respectively. N is the total number of the simulations for comparisons, and $\bar{O}$ donates the average of the observation. The IOA ranges from 0 to 1, with 1 showing a perfect agreement of the simulation with the observation.

3 Results and discussions

3.1 Model evaluation

3.1.1 Meteorological parameters simulations in Beijing

Considering the key role of meteorological conditions in air pollution simulations (Bei et al., 2012, 2017), Figure 2 shows the temporal profiles of observed and simulated TSFC, RH, wind speed and wind direction from 04 to 15 July 2015 at the weather station in Beijing (Figure 1). The WRF-Chem model generally well replicates the temporal variation of the TSFC during the whole episode compared to observations, with the MB and IOA of 0.7°C and 0.95, respectively. The model considerably overestimates TSFC on July 4 and in the evening of July 13 and 14. The model also performs reasonably well in simulating the RH against observations, with the MB and IOA of -5.3% and 0.84, respectively. The observed high RH exceeding 75% during nighttime is generally well captured, except on July 4 and 14 when the TSFC is overestimated. In addition, the model also reasonably well tracks the temporal variations of the wind speed and direction compared to observations, with an IOA of around 0.60. In general, the reasonable simulations of meteorological fields provide a reliable basis for modeling the O_3 and $PM_{2.5}$ pollution episode in the present study.

3.1.2 Air pollutant simulations in BTH

Figure 3 shows the diurnal profiles of measured and simulated $PM_{2.5}$, O_3, NO_2, SO_2, and CO mass concentrations averaged over all ambient monitoring stations in BTH during the episode. Apparently, the WRF-Chem model exhibits good performance in simulating the temporal variations of $PM_{2.5}$ and O_3 mass concentrations against observations in BTH, with the IOAs of around 0.90. However, the model fails to capture the observed high $PM_{2.5}$ concentration on July 11 and 12, and frequently overestimates O_3 concentration in the evening, with a MB of 1.2 μg m^{-3}. The simulated temporal variation of NO_2 mass concentrations is also generally consistent with observations in BTH, but the model frequently overestimates NO_2 concentrations against observations during nighttime, which

might be caused by the low simulated planetary boundary layer (PBL) height or the O_3 overestimation. Simulations of the SO_2 mass concentration are not as good as those of other pollutants in BTH during the episode, with an IOA of 0.45. During summertime, SO_2 is principally emitted by the point source, including the power plants and agglomerated industrial zones, so the uncertainties of simulated wind fields substantially affect the SO_2 simulations. Additionally, the model overestimation of SO_2 concentrations is also considerable during nighttime, which is perhaps due to the simulated low PBL height. It is worth noting that NH_3 plays an important role in the sulfate formation (Wang et al., 2016; Cheng et al., 2016), so it is imperative to validate NH_3 simulations using measurements. However, due to lack of routine measurements of NH_3 in BTH, the validation of the NH_3 simulation is not provided in the study.

Figure 4 presents the distributions of simulated and observed near-surface mass concentrations of $PM_{2.5}$, O_3, NO_2 and SO_2 along with the simulated wind fields averaged from 04 to 15 July 2015. Generally, the simulated wind in BTH is weak during the episode and the easterly wind prevails, which is favorable for the accumulation of air pollutants, particularly along the Taihang and Yanshan Mountains due to the blocking effect. The model generally well reproduces the spatial distribution of $PM_{2.5}$ concentrations against observations, with the $PM_{2.5}$ concentration exceeding 35 μg m^{-3} in the plain area of BTH (Figure 4a). The average simulated peak O_3 concentrations are more than 200 μg m^{-3} during the episode in the plain area of BTH, consistent with the measurement and showing the severe O_3 pollution (Figure 4b). High levels of O_3 indicate a strong atmospheric oxidation capacity (AOC), facilitating the photochemical reactions over BTH (Figure 4b). The simulated high NO_2 and SO_2 concentrations are generally concentrated in cities and their surrounding areas, in agreement with the measurement (Figures 4c and 4d). However, the model considerably overestimates the NO_2 concentrations against the measurement in Beijing,

Shijiazhuang and Handan city. In addition, the SO_2 concentrations in BTH are much lower than those during wintertime (Li et al., 2018; Xing et al., 2019), generally less than 30 μg m^{-3}. Reduced SO_2 concentrations in BTH during summertime are caused by the efficient removal of gas-phase oxidations due to the high AOC, the reduction of residential coal combustion, and the increased PBL height.

3.1.3 Aerosol species simulations in Beijing

Figure 5 presents the temporal variations of simulated and observed submicron nitrate, ammonium, SOA and POA mass concentrations at NCNST site in Beijing from 04 to 15 July 2015. The WRF-Chem model reasonably reproduces the diurnal variation of the nitrate concentration compared to observations, with the MB and IOA of -0.7 μg m^{-3} and 0.81, respectively (Figure 5a). Nitrate formation is sensitive to the air temperature, and its variation is generally negatively correlated with that of the temperature. When the temperature is lowest in the early morning, the nitrate concentration reaches its peaks; when the temperature is up to 30°C in the afternoon, the nitrate concentration is generally less than 1 μg m^{-3}. The simulated ammonium profile is generally in agreement with observations, with an IOA of 0.71, but the model biases are still large. The model underestimation of the ammonium concentration is considerable on July 11 and 12, and the overestimation is also noticeable on July 6 and 7. The model reasonably reproduces the temporal variation of the SOA and POA concentrations compared to the measurement at the NCNST site, with the IOA of around 0.60. The observed SOA concentration exhibits rather large fluctuations from 11 to 15 July 2015, which are not well tracked by the model. The model fails to capture the observed large fluctuations of POA concentrations. The POA concentration in Beijing is primarily contributed by direct emissions from vehicles, cooking, coal combustion, biomass burning, and trans-boundary transport from outside of Beijing (Wu et al., 2017; Wu et al., 2018), and

the uncertainties in various anthropogenic sources and simulated meteorological fields substantially affect the POA simulations (Bei at al., 2017; Bei et al., 2016).

In summary, the WRF-CHEM model performs reasonably well in simulating meteorological fields, air pollutants and aerosol species, providing the underlying basis for further evaluation of the sulfate formation pathway.

3.2 Contributions of four pathways to sulfate formation in Beijing and BTH

Figure 6a provides the diurnal profile of simulated and observed submicron sulfate concentrations at NCNST site in Beijing from 04 to 15 July 2015. The model reasonably well tracks temporal variations of the observed sulfate concentration, with the MB and IOA of -0.9 μg m^{-3} and 0.71, respectively. During 11 to 12 July 2015, the model noticeably underestimates the high sulfate concentrations against the measurement. As mentioned in Section 2, the aqueous oxidation of SO_2 in cloud or fog droplets is not considered in the simulation, which might constitute one of the most possible reasons for the underestimation.

Figures 6b-e present the contributions of the four pathways to the sulfate formation during the episode at NCNST site in Beijing. On average, the HR_SO_2 plays the most important role in the sulfate formation, with a contribution of about 32.1% (Figure 6b). Li et al. (2017) have also shown that the HR_SO_2 is the dominant sulfate source, contributing around 58.4% to sulfate concentrations in Beijing during wintertime due to the very humid conditions and inefficient sulfate formation from gas-phase SO_2 oxidation due to the low AOC. In this study, the average simulated RH is not high in Beijing, less than 50% during the episode, and high O_3 concentrations enhance the AOC to facilitate the gas-phase SO_2 oxidation, causing the decreased sulfate contribution of the HR_SO_2. It is worth nothing that the HR_SO_2 relies on the assumption that alkalinity is sufficient to maintain the high iron-catalyzed reaction rate (Li et al., 2017). Figure 7 presents the temporal variation of the average simulated aqueous pH in Beijing during the episode. The simulated pH generally

fluctuates between 5 and 7, with an average of 6.2, warranting the efficient iron-catalyzed reaction involving aerosol water. High O_3 concentrations substantially increase the sulfate formation efficiency through the SO_2 oxidation by OH and sCI. The OH_SO_2 plays considerable roles in the sulfate formation, with the contribution of 30.8% (Figure 6c). It is worth noting that the primary emission pathway contributes 24.0% of the sulfate concentration at NCNST site.

The sCI_SO_2 accounts for about 13.1% of sulfate concentrations at NCNST site, less than the contribution of the other three pathways. Effects of the sCI_SO_2 on the sulfate formation depend on the κ_{sCI+SO_2}. The reported κ_{sCI+SO_2} from previous studies spans orders of magnitude (Welz et al., 2012; Maudlin et al., 2012; Jenkin et al., 1997). In the present study, an upper limit of the κ_{sCI+SO_2} (3.9×10^{-11} cm^3 s^{-1}) is used in the B-case, which is reported by Welz et al. (2012). Furthermore, the reaction of sCI with H_2O is the main loss pathway for sCI in the atmosphere, and the κ_{sCI+H_2O} used in this study represents a lower limit (1.97×10^{-18} cm^3 s^{-1}) (Ying et al., 2014). Therefore, the contribution of the sCI_SO_2 to the sulfate formation might be overestimated in the present study.

Figure 8 presents the spatial distribution of contributions of the four pathways to the sulfate formation averaged during the episode. The contribution of the HR_SO_2 to the sulfate formation is substantial in BTH, particularly in the plain area with the sulfate contribution exceeding 4.0 μg m^{-3} and being up to 7.0 μg m^{-3} (Figure 8a). Under the condition of high O_3 concentrations, the OH_SO_2 oxidation also becomes an important sulfate source, with a sulfate contribution of more than 3.0 μg m^{-3} in the plain area of BTH, which is comparable to the heterogeneous pathway (Figure 8b). Similar to the spatial distribution of SO_2 concentrations, the sulfate contribution of the primary emission is mainly concentrated in cities and their downwind areas (Figure 4c). In the plain area of BTH, the sulfate contribution of the primary emission is more than 2.0 μg m^{-3} on average, and exceeds 7 μg m^{-3} in

highly-industrialized cities, such as Shijiazhuang, Tangshan and Xingtai. The sulfate contribution of the sCI_SO_2 is not as important as the other three sources, more than 0.8 μg m^{-3} in the plain area of BTH, and the most striking in Beijing, with a contribution exceeding 1.2 μg m^{-3}.

3.3 Sensitivity studies

Considering the large variation of the reported κ_{sCI+SO_2} and the importance of water vapor in the sCI removal, sensitivity studies are further conducted to evaluate the sulfate contribution of the sCI_SO_2 in BTH when the different κ_{sCI+SO_2} and κ_{sCI+H_2O} are used in simulations. In the B-case simulation, an upper limit of the κ_{sCI+SO_2} and a lower limit of κ_{sCI+H_2O} are used. The simulated average sulfate concentration is 10.8 μg m^{-3} in BTH, constituting a major component of $PM_{2.5}$. The HR_SO_2 and OH_SO_2 constitute the two most important sulfate sources, with the sulfate contribution of 35% and 33%, respectively. The primary emission makes up about 23% of the sulfate in BTH, caused by high SO_2 emissions. The sulfate contribution of the sCI_SO_2 is about 1.0 μg m^{-3} or 9.1%, less than that in Beijing with the higher O_3 concentration. Pierce et al. (2013) have used the same κ_{sCI+SO_2} in GEOS-CHEM model as the B-case in the study, revealing that the H_2SO_4 concentration is increased by 4% due to the sCI_SO_2 on global average. The H_2SO_4 enhancement is 10-25% over forested regions in the Northern Hemisphere (up to 100% in July), but is generally negligible elsewhere. The sulfate contribution of the sCI_SO_2 in BTH is close to those over forested regions in Pierce et al. (2013), which is primarily caused by the increasing trend of O_3 and the high precursors emissions of sCI, such as ethene, isoprene and monoterpenes during summertime in the region. Additionally, Boy et al. (2013) have employed the κ_{sCI+SO_2} reported by Mauldin et al. (2012) and Welz et al. (2012) to verify the sulfate contribution of the sCI_SO_2 in European, showing a H_2SO_4 contribution of as much as 33-46% at the ground level. These different sulfate contributions of the sCI_SO_2 are mainly caused by

the variation of the reaction constant of sCI with SO_2, NO_2, and H_2O and the sCI precursors concentration, as well as the atmospheric conditions in simulations (Taatjes, 2017).

Although the sCI_SO_2 is not an important sulfate source, its contribution might be overestimated. The κ_{sCI+SO_2} used in the B-case is only measured for the smallest sCI, H_2COO, but the larger sCI (such as those produced from typical larger alkenes in the atmosphere) might have a lower reaction rate with SO_2, and produce stable low volatilities species such as sulfur-bearing secondary ozonides (Spracklen et al., 2011; Vereecken et al., 2012). Additionally, Welz et al. (2012) have measured κ_{sCI+SO_2} at low pressure (4 Torr), making it unclear if those rates are appropriate for atmospheric conditions.

In the S1-case, the reported κ_{sCI+SO_2} (6.0×10^{-13} cm^3 s^{-1}) by Mauldin et al. (2012) is used, which is deduced from ozonolysis of α-pinene under boundary-layer atmospheric conditions, and the κ_{sCI+H_2O} and κ_{sCI+NO_2} are the same as those in the B-case. The sulfate contribution of the sCI_SO_2 becomes insignificant, around 0.3 μg m^{-3} or less than 3% of the total simulated sulfate concentration on average during the episode in BTH (Figure 9). Compared to the B-case, the sulfate contribution of the sCI_SO_2 is decreased by more than 70% in the S1-case. The substantial reduction reveals that further studies are needed to precisely determine the κ_{sCI+SO_2}.

One of the largest uncertainties concerning the lifetime of sCI is related to the κ_{sCI+H_2O}, but few studies have been conducted to directly measure the κ_{sCI+H_2O}. The reported κ_{sCI+H_2O} varies widely, ranging from 2×10^{-19} to 1×10^{-15} cm^3 s^{-1} (Hatakeyama and Akimoto 1994), and several studies show that the κ_{sCI+H_2O} needs to be adjusted when the κ_{sCI+SO_2} is adjusted (Li et al., 2013; Calvert et al., 1978; Suto et al., 1985). In order to evaluate the effect of water vapor on the sCI_SO_2, in the S2-case, the κ_{sCI+H_2O} is increased to 2.4×10^{-15} cm^3 s^{-1} based on the reported ratio of κ_{sCI+H_2O} to κ_{sCI+SO_2} (6.1×10^{-5}) (Calvert et al., 1978), and the

κ_{sCI+SO_2} and κ_{sCI+NO_2} are the same as those in the B-case. The average sulfate contribution of the sCI_SO_2 in BTH is decreased to 0.2 μg m^{-3} or less than 2% of the total simulated sulfate concentration due to the competition of water vapor with SO_2 for sCI (Figure 9). Additionally, if a low κ_{sCI+SO_2} is used in the S2-case, the effect of water vapor on the sCI removal becomes more substantial.

4 Summaries and Conclusion

In the present study, a persistent air pollution episode with high O_3 and $PM_{2.5}$ concentrations from 04 to 15 July 2015 in BTH is simulated using a source-oriented WRF-Chem model to study the contributions of four pathways to the sulfate formation. The four sulfate formation pathways include the heterogeneous reaction of SO_2 involving aerosol water (HR_SO_2), the SO_2 oxidation by OH (OH_SO_2), the primary emission, and the SO_2 oxidation by sCI (sCI_SO_2).

The WRF-Chem model reasonably reproduces the temporal variations of the meteorological parameters compared to observations at the weather station in Beijing. The model performs reasonably well in simulating the temporal profiles and spatial distributions of air pollutant mass concentrations against observations at monitoring sites in BTH. In addition, the simulated diurnal variations of submicron nitrate, ammonium, POA, SOA, and sulfate mass concentrations are generally in good agreements with the measurements at NCNST site in Beijing.

On average in BTH during the simulation episode, the HR_SO_2 plays the most important role in the sulfate formation, with a sulfate contribution of about 35%. Under conditions with the high O_3 concentration during summertime, the OH_SO_2 also constitutes a major sulfate source comparable to the HR_SO_2, accounting for about 33% of the total simulated sulfate concentration in BTH. Due to high SO_2 emissions, the primary emission

contributes about 23% of the sulfate concentration in BTH, mainly concentrated in cities and their downwind regions.

When an upper limit of the κ_{sCI+SO_2} (3.9×10^{-11} cm^3 s^{-1}) and a lower limit of κ_{sCI+H_2O} (1.97×10^{-18} cm^3 s^{-1}) are used, the sCI_SO_2 plays an appreciable role in the sulfate formation, with a contribution of around 9%. However, there still exist large uncertainties in contributions of the sCI_SO_2 to the sulfate formation. Sensitivity studies reveal that the sulfate contribution of the sCI_SO_2 is substantially decreased to less than 3%, when the κ_{sCI+SO_2} is decreased to 6.0×10^{-13} cm^3 s^{-1} but the lower limit of κ_{sCI+H_2O} remains. Furthermore, when the κ_{sCI+H_2O} is increased to 2.38×10^{-15} cm^3 s^{-1} based on the reported ratio of κ_{sCI+H_2O} to κ_{sCI+SO_2} (6.1×10^{-5} cm^3 s^{-1}) but the upper limit of the κ_{sCI+SO_2} remains, the sulfate contribution of the reaction becomes insignificant, less than 2%. Future studies still need to be conducted to measure the κ_{sCI+SO_2} and κ_{sCI+H_2O} under the atmospheric condition to better evaluate effects of the sCI chemistry on the sulfate formation.

Author contribution. Guohui Li, as the contact author, provided the ideas and financial support, verified the conclusions, and revised the paper. Lang Liu conducted a research, designed the experiments, carried the methodology out, performed the simulation, processed the data, prepared the data visualization, and prepared the manuscript with contributions from all authors. Naifang Bei, Jiarui Wu and Xia Li provided the treatment of meteorological data, analyzed the study data, validated the model performance, and reviewed the manuscript. Suixin Liu, Qingchuan Yang, Tian Feng, and Jiamao Zhou provided the observation data used in the study, synthesized the observation, and reviewed the paper. Xuexi Tie and Junji Cao provided critical reviews pre-publication stage.

Acknowledgements. This work is financially supported by the National Key R&D Plan (Quantitative Relationship and Regulation Principle between Regional Oxidation Capacity of Atmospheric and Air Quality (2017YFC0210000)) and National Research Program for Key Issues in Air Pollution Control (DQGG0105).

References

Anglada, J. M., González, J., Torrent-Sucarrat, M.: Effects of the substituents on the reactivity of carbonyl oxides. A theoretical study on the reaction of substituted carbonyl oxides with water, Phys. Chem. Chem. Phys., 13(28), 13034-13045, https://doi.org/10.1039/C1CP20872A, 2011.

Bei, N., Li, G., Huang, R.-J., Cao, J., Meng, N., Feng, T., Liu, S., Zhang, T., Zhang, Q., and Molina, L. T.: Typical synoptic situations and their impacts on the wintertime air pollution in the Guanzhong basin, China, Atmos. Chem. Phys., 16, 7373-7387, doi: 10.5194/acp-16-7373-2016, 2016.

Bei, N., Li, G., and Molina, L. T.: Uncertainties in SOA sim- ulations due to meteorological uncertainties in Mexico City during MILAGRO-2006 field campaign, Atmos. Chem. Phys., 12, 11295–11308, https://doi.org/10.5194/acp-12-11295-2012, 2012.

Bei, N., Wu, J., Elser, M., Feng, T., Cao, J., El-Haddad, I., Li, X., Huang, R., Li, Z., Long, X., Xing, L., Zhao, S., Tie, X., Pr v t, A. S. H., and Li, G.: Impacts of meteorological uncertainties on the haze formation in Beijing-Tianjin-Hebei (BTH) during wintertime: a case study, Atmos. Chem. Phys., 17, 14579-14591, doi: 10.5194/acp-17-14579-2017, 2017.

Binkowski, F. S. and Roselle, S. J.: Models-3 Community Multiscale Air Quality (CMAQ) model aerosol component 1. Model description, J. Geophys. Res.-Atmos., 108, 335-346, https://doi.org/10.1029/2001JD001409, 2003.

Boy, M., Mogensen, D., Smolander, S., Zhou, L., Nieminen, T., Paasonen, P., Plass-Dülmer, C., Sipilä, M., Petäjä, T., Mauldin, L., Berresheim, H., and Kulmala, M.: Oxidation of SO_2 by stabilized Criegee intermediate (sCI) radicals as a crucial source for atmospheric sulfuric acid concentrations, Atmos. Chem. Phys., 13, 3865-3879, https://doi.org/10.5194/acp-13-3865-2013, 2013.

Calvert, J. G., Su, F., Bottenheim, J. W., and Strausz, O. P.: Mechanism of the homo-geneous oxidation of sulfur dioxide in the troposphere, Atmos. Environ., 12, 197-226, 1978.

Chen, F. and Dudhia, J.: Coupling an advanced land surface-hydrology model with the Penn State-NCAR MM5 modeling system. Part I: Model implementation and sensitivity, Mon. Weather Rev., 129, 569-585, https://doi.org/10.1175/1520-0493(2001)129<0569:CAALSH>2.0.CO;2, 2001.

Cheng, Y., Zheng, G., Wei, C., Mu, H., Zheng, B., Wang, Z., Gao, M., Zhang, Q., He, K., Carmichael, G., Pöschl, U., and Su, H.: Reactive nitrogen chemistry in aerosol water as a source of sulfate during haze events in China, Sci. Adv., 2(12), e1601530, DOI: 10.1126/sciadv.1601530, 2016.

Chou, M. D. and Suarez, M. J.: A solar radiation parameterization for atmospheric studies, NASA TM-104606, Nasa Tech. memo 15, 1999.

Chou, M. D., Suarez, M. J., Liang, X. Z., Yan, M. H., and Cote, C.: A Thermal Infrared Radiation Parameterization for Atmospheric Studies, NASA TM-2001-104606, Max J., 19, 2001.

Cox, R. A., and Penkett, S. A.: Oxidation of atmospheric SO_2 by products of the Ozone-Olefin reaction, Nature, 230, 321-322, 1971.

Dunker, A. M., Morris, R. E., Pollack, A. K., Schleyer, C. H., and Yarwood, G: Photochemical modeling of the impact of fuels and vehicles on urban ozone using auto oil program data, Environ. Sci. Technol., 30, 787–801, https://doi.org/10.1021/es950175m, 1996.

Feng, T., Li, G., Cao, J., Bei, N., Shen, Z., Zhou, W., Liu, S., Zhang, T., Wang, Y., Huang, R.-J., Tie, X., and Molina, L. T.: Simulations of organic aerosol concentrations during springtime in the Guanzhong Basin, China, Atmos. Chem. Phys., 16, 10045-10061, https://doi.org/10.5194/acp-16-10045-2016, 2016.

Gao, M., Carmichael, G. R., Wang, Y., Saide, P. E., Yu, M., Xin, J., Liu, Z., and Wang, Z.: Modeling study of the 2010 regional haze event in the North China Plain, Atmos. Chem. Phys., 16, 1673-1691, https://doi.org/10.5194/acp-16-1673-2016, 2016.

Grell, G. A., Peckham, S. E., Schmitz, R., McKeen, S. A., Frost, G., Skamarock, W. C., and Eder, B.: Fully coupled "online" chemistry within the WRF model, Atmos. Environ., 39, 6957–6975, 2005.

Guenther, A., Karl, T., Harley, P., Wiedinmyer, C., Palmer, P. I., and Geron, C.: Estimates of global terrestrial isoprene emissions using MEGAN (Model of Emissions of Gases and Aerosols from Nature), Atmos. Chem. Phys., 6, 3181–3210, https://doi.org/10.5194/acp-6-3181-2006, 2006.

Guo, S., Hu, M., Zamora, M. L., Peng, J., Shang, D., Zheng, J., Du, Z., Wu, Z., Shao, M., and Zeng, L.: Elucidating severe urban haze formation in China, P. Natl. Acad. Sci. USA, 111, 17373-17378, https://doi.org/10.1073/pnas.1419604111, 2014.

Hatakeyama, S. and Akimoto, H.: Reactions of Criegee Intermedi- ates in the gas phase, Res. Chem. Intermed., 20, 503–524, 1994.

He, P., Alexander, B., Geng, L., Chi, X., Fan, S., Zhan, H., Kang, H., Zheng, G., Cheng, Y., Su, H., Liu, C., and Xie, Z.: Isotopic constraints on heterogeneous sulfate production in Beijing haze, Atmos. Chem. Phys., 18, 5515-5528, https://doi.org/10.5194/acp-18-5515-2018, 2018.

Hong, S. Y. and Lim, J. O. J.: The WRF Single-Moment 6-Class Microphysics Scheme (WSM6), Asia-Pacif. J. Atmos. Sci., 42, 129-151, 2006.

Horowitz, L. W., Walters, S., Mauzerall, D. L., Emmons, L. K., Rasch, P. J., Granier, C., Tie, X., Lamarque, J. F., Schultz, M. G., Tyndall, G. S., Orlando, J. J., and Brasseur, G. P.: A global simulation of tropospheric ozone and related tracers: Description and evaluation of MOZART, version 2, J. Geophys. Res.-Atmos., 108, 4784, https://doi.org/10.1029/2002JD002853, 2003.

Janjić, Z. I.: Nonsingular Implementation of the Mellor-Yamada Level 2.5 Scheme in the NCEP Meso Model, NCEP Office Note 437, 2002.

Jenkin, M. E., Saunders, S. M., and Pilling, M. J.: The tropo- spheric degradation of volatile organic compounds: a proto- col for mechanism development, Atmos. Environ., 31, 81-104, doi:10.1016/S1352-2310(96)00105-7, 1997.

Li, G., Bei, N., Cao, J., Huang, R., Wu, J., Feng, T., Wang, Y., Liu, S., Zhang, Q., Tie, X., and Molina, L. T.: A possible pathway for rapid growth of sulfate during haze days in China, Atmos. Chem. Phys., 17, 3301-3316, https://doi.org/10.5194/acp-17-3301-2017, 2017.

Li, G., Bei, N., Tie, X., and Molina, L. T.: Aerosol effects on the photochemistry in Mexico City during MCMA-2006/MILAGRO campaign, Atmos. Chem. Phys., 11, 5169-5182, https://doi.org/10.5194/acp-11-5169-2011, 2011a.

Li, G., Lei, W., Bei, N., and Molina, L. T.: Contribution of garbage burning to chloride and $PM_{2.5}$ in Mexico City, Atmos. Chem. Phys. 12, 8751-8761, https://doi.org/10.5194/acp-12-8751-2012, 2012.

Li, G., Lei, W., Zavala, M., Volkamer, R., Dusanter, S., Stevens, P., and Molina, L. T.: Impacts of HONO sources on the photochemistry in Mexico City during the MCMA-2006/MILAGO Campaign, Atmos. Chem. Phys., 10, 6551-6567, https://doi.org/10.5194/acp-10-6551-2010, 2010.

Li, G., Zavala, M., Lei, W., Tsimpidi, A. P., Karydis, V. A., Pandis, S. N., Canagaratna, M. R., and Molina, L. T.: Simulations of organic aerosol concentrations in Mexico City using the WRF-CHEM model during the MCMA-2006/MILAGRO campaign, Atmos. Chem. Phys., 11, 3789-3809, https://doi.org/10.5194/acp-11-3789-2011, 2011b.

Li, G., Zhang, R., Fan, J., and Tie, X.: Impacts of black carbon aerosol on photolysis and ozone, J. Geophys. Res.-Atmos., 110, D23206, https://doi.org/10.1029/2005JD005898, 2005.

Li, J., Ying, Q., Yi, B., and Yang, P.: Role of stabilized Criegee Intermediates in the formation of atmospheric sulfate in eastern United States, Atmos. Environ., 79, 442-447, http://dx.doi.org/10.1016/j.atmosenv.2013.06.048, 2013.

Li, X., Wu, J., Elser, M., Feng, T., Cao, J., El-Haddad, I., Huang, R., Tie, X., Prévôt, A. S. H., and Li, G.: Contributions of residential coal combustion to the air quality in Beijing–Tianjin–Hebei (BTH), China: a case study, Atmos. Chem. Phys., 18, 10675-10691, https://doi.org/10.5194/acp-18-10675-2018, 2018.

Mauldin, R. L., Berndt, T., Sipilä, M., Paasonen, P., Petäjä, T., Kim, S., Kurtén, T., Stratmann, F., Kerminen, V. M., and Kulmala, M.: A new atmospherically relevant oxidant of sulphur dioxide, Nature, 488, 193-196, doi:10.1038/nature11278, 2012.

Nenes, A., Pandis, S. N., and Pilinis, C.: ISORROPIA: A new thermodynamic equilibrium model for multiphase multicomponent inorganic aerosols, Aquat. Geochem., 4, 123–152, https://doi.org/10.1023/a:1009604003981, 1998.

Percival, C. J., Welz, O., Eskola, A. J., Savee, J. D., Osborn, D. L., Topping, D. O., Lowe, D., Utembe, S. R., Cooke, M. C., Taatjes, C. A., and Shallcross, D. E.: Regional and global impacts of Criegee intermediates on atmospheric sulphuric acid concentrations and first steps of aerosol formation, Faraday discussions, 165, 45-73, 2013.

Pierce, J. R., Evans, M. J., Scott, C. E., D'Andrea, S. D., Farmer, D. K., Swietlicki, E., and Spracklen, D. V.: Weak global sensitivity of cloud condensation nuclei and the aerosol indirect effect to Criegee + SO_2 chemistry, Atmos. Chem. Phys., 13, 3163-3176, https://doi.org/10.5194/acp-13-3163-2013, 2013.

Sarwar, G., Fahey, K., Kwok, R., Gilliam, R. C., Roselle, S. J., Mathur, R., Xue, J., Yu, J., and Carter, W. P.: Potential impacts of two SO_2 oxidation pathways on regional sulfate concentrations: Aqueous-phase oxidation by NO_2 and gas-phase oxidation by Stabilized Criegee Intermediates, Atmos. Environ., 68, 186-197, https://doi.org/10.1016/j.atmosenv.2012.11.036, 2013.

Sarwar, G., Simon, H., Fahey, K., Mathur, R., Goliff, W. S., and Stockwell, W. R.: Impact of sulfur dioxide oxidation by Stabilized Criegee Intermediate on sulfate, Atmos. Environ., 85, 204-214, https://doi.org/10.1016/j.atmosenv.2013.12.013, 2014.

Seinfeld, J. H. and Pandis, S. N.: Atmospheric Chemistry and Physics: From Air Pollution to Climate Change, 2nd Edn., John Wiley & Sons Inc., New York, 2006.

Spracklen, D. V., Jimenez, J. L., Carslaw, K. S., Worsnop, D. R., Evans, M. J., Mann, G. W., Zhang, Q., Canagaratna, M. R., Allan, J., Coe, H., McFiggans, G., Rap, A., and Forster, P.: Aerosol mass spectrometer constraint on the global secondary organic aerosol budget, Atmos. Chem. Phys., 11, 12109-12136, https://doi.org/10.5194/acp-11-12109-2011, 2011.

Sun, Y. L., Wang, Z. F., Du, W., Zhang, Q., Wang, Q. Q., Fu, P. Q., Pan, X. L., Li, J., Jayne, J., and Worsnop, D. R.: Long-term real-time measurements of aerosol particle composition in Beijing, China: seasonal variations, meteorological effects, and source analysis, Atmos. Chem. Phys., 15, 10149-10165, https://doi.org/10.5194/acp-15-10149-2015, 2015.

Suto, M., Manzanares, E. R., and Lee, L. C.: Detection of sulfuric-acid aerosols by ultraviolet scattering. Environ. Sci. Tech., 19, 815-820, 1985.

Taatjes, C. A.: Criegee intermediates: What direct production and detection can teach us about reactions of carbonyl oxides, Annu. Rev. Phys. Chem. 2017. 68:183–207, 2017.

Tao, J., Zhang, L., Cao, J., and Zhang, R.: A review of current knowledge concerning $PM_{2.5}$ chemical composition, aerosol optical properties and their relationships across China, Atmos. Chem. Phys., 17, 9485-9518, https://doi.org/10.5194/acp-17-9485-2017, 2017.

Tie, X., Madronich, S., Walters, S., Zhang, R., Rasch, P., and Collins, W.: Effect of clouds on photolysis and oxidants in the troposphere, J. Geophys. Res.-Atmos., 108, 4642, https://doi.org/10.1029/2003JD003659, 2003.

Vereecken, L., Harder, H., and Novelli, A.: The reaction of Criegee intermediates with NO, RO_2, and SO_2, and their fate in the atmosphere, Phys. Chem. Chem. Phys., 14, 14682–14695, doi:10.1039/c2cp42300f, 2012.

Wang, S., and Hao, J.: Air quality management in China: Issues, challenges, and options, J. Environ. Sci., 24, 2-13, 2012.

Wang, G., Zhang, R., Gomez, M. E., Yang, L., Levy Zamora, M., Hu, M., Lin, Y., Peng, J., Guo, S., Meng, J., Li, J., Cheng, C., Hu, T., Ren, Y., Wang, Y., Gao, J., Cao, J., An, Z., Zhou, W., Li, G., Wang, J., Tian, P., Marrero-Ortiz, W., Secrest, J., Du, Z., Zheng, J., Shang, D., Zeng, L., Shao, M., Wang, W., Huang, Y., Wang, Y., Zhu, Y., Li, Y., Hu, J., Pan, B., Cai, L., Cheng, Y., Ji, Y., Zhang, F., Rosenfeld, D., Liss, P. S., Duce, R. A., Kolb, C. E., and Molina, M. J.: Persistent sulfate formation from London Fog to Chinese haze, P. Natl. Acad. Sci. USA, 113(48), 13630-13635, https://doi.org/10.1073/pnas.1616540113, 2016.

Welz, O., Savee, J. D., Osborn, D. L., Vasu, S. S., Percival, C. J., Shallcross, D. E., and Taatjes, C.A: Direct kinetic measurements of Criegee Intermediate (CH_2OO) formed by reaction of CH_2I with O_2, Science, 335, 204-207, doi:10.1126/science.1213229, 2012.

Wesely, M. L.: Parameterization of surface resistances to gaseous dry deposition in regional-scale numerical models, Atmos. Environ., 23, 1293-1304, https://doi.org/10.1016/0004-6981(89)90153-4, 1989.

Wu, J., Li, G., Cao, J., Bei, N., Wang, Y., Feng, T., Huang, R., Liu, S., Zhang, Q., and Tie, X.: Contributions of trans-boundary transport to summertime air quality in Beijing, China, Atmos. Chem. Phys., 17, 2035-2051, https://doi.org/10.5194/acp-17-2035-2017, 2017.

Wu, J., Bei, N., Li, X., Cao, J., Feng, T., Wang, Y., Tie, X., and Li, G.: Widespread air pollutants of the North China Plain during the Asian summer monsoon season: a case study, Atmos. Chem. Phys., 18, 8491-8504, https://doi.org/10.5194/acp-18-8491-2018, 2018.

Xing, L., Wu, J., Elser, M., Tong, S., Liu, S., Li, X., Liu, L., Cao, J., Zhou, J., El-Haddad, I., Huang, R., Ge, M., Tie, X., Prévôt, A. S. H., and Li, G.: Wintertime secondary organic aerosol formation in Beijing–Tianjin–Hebei (BTH): contributions of HONO sources and heterogeneous reactions, Atmos. Chem. Phys., 19, 2343-2359, https://doi.org/10.5194/acp-19-2343-2019, 2019.

Ying Q., Cureno, I. V., Chen, G., Ali, S., Zhang, H., Malloy, M., Bravo, H. A., and Sosa, R.: Impacts of stabilized Criegee Intermediates, surface uptake processes and higher aromatic secondary organic aerosol yields on predicted $PM_{2.5}$ concentrations in the Mexico City Metropolitan Zone, Atmos. Environ., 94, 438-447, http://dx.doi.org/10.1016/j.atmosenv.2014.05.056, 2014.

Ying, Q. and Kleeman, M. J.: Source contributions to the regional distribution of secondary particulate matter in California, Atmos. Environ., 40: 736-752, https://doi.org/10.1016/j.atmosenv.2005.10.007, 2006.

Ying, Q. and Krishnan, A.: Source contribution of volatile organic compounds to ozone formation in southeast Texas, J. Geophys. Res.-Atmos., 115, D17306, https://doi.org/10.1029/2010JD013931, 2010.

Zhang, H. and Ying, Q.: Secondary organic aerosol formation and source apportionment in Southeast Texas, Atmos. Environ., 45: 3217-3227, https://doi.org/10.1016/j.atmosenv.2011.03.046, 2011.

Zhang, Q., Streets, D. G., Carmichael, G. R., He, K., Huo, H., Kannari, A., Klimont, Z., Park, I. S., Reddy, S., Fu, J., Chen, D., Duan, L., Lei, Y.,Wang, L., and Yao, Z.: Asian emissions in 2006 for the NASA INTEX-B mission, Atmos. Chem. Phys., 9, 5131-5153, https://doi.org/10.5194/acp-9-5131-2009, 2009.

Zhang, X. Y., Wang, Y. Q., Niu, T., Zhang, X. C., Gong, S. L., Zhang, Y. M., and Sun, J. Y.: Atmospheric aerosol compositions in China: spatial/temporal variability, chemical signature, regional haze distribution and comparisons with global aerosols, Atmos. Chem. Phys., 12, 779-799, https://doi.org/10.5194/acp-12-779-2012, 2012.

Zhao, P. S., Dong, F., He, D., Zhao, X. J., Zhang, X. L., Zhang, W. Z., Yao, Q., and Liu, H. Y.: Characteristics of concentrations and chemical compositions for $PM_{2.5}$ in the region of Beijing, Tianjin, and Hebei, China, Atmos. Chem. Phys., 13, 4631-4644, https://doi.org/10.5194/acp-13-4631-2013, 2013.

Atmos. Chem. Phys. Discuss., https://doi.org/10.5194/acp-2019-313
Manuscript under review for journal Atmos. Chem. Phys.
Discussion started: 13 May 2019

Table 1 WRF-CHEM model configurations.

Regions	Beijing-Tianjin-Hebei (BTH)
Simulation period	July 4 to 15, 2015
Domain size	300 × 300
Domain center	38.0°N, 116.0°E
Horizontal resolution	6km × 6km
Vertical resolution	35 vertical levels with a stretched vertical grid with spacing ranging from 30m near the surface, to 500m at 2.5km and 1km above 14km
Microphysics scheme	WSM 6-class graupel scheme (Hong and Lim, 2006)
Boundary layer scheme	MYJ TKE scheme (Janjić, 2002)
Surface layer scheme	MYJ surface scheme (Janjić, 2002)
Land-surface scheme	Unified Noah land-surface model (Chen and Dudhia, 2001)
Long-wave radiation scheme	Goddard longwave scheme (Chou and Suarez, 2001)
Short-wave radiation scheme	Goddard shortwave scheme (Chou and Suarez, 1999)
Meteorological boundary and initial conditions	ERA-Interim 0.125°×0.125° reanalysis data (http://apps.ecmwf.int/datasets)
Chemical initial and boundary conditions	MOZART 6-hour output (Horowitz et al., 2003) (https://www.acom.ucar.edu/wrf-chem/mozart.shtml)
Anthropogenic emission inventory	SAPRC-99 chemical mechanism emissions (Zhang et al., 2009)
Biogenic emission inventory	MEGAN model developed by Guenther et al. (2006)
Four-dimension data assimilation	NCEP ADP Global Air Observational Weather Data (https://rda.ucar.edu/datasets)
Model spin-up time	24 hours

Atmos. Chem. Phys. Discuss., https://doi.org/10.5194/acp-2019-313
Manuscript under review for journal Atmos. Chem. Phys.
Discussion started: 13 May 2019

Table 2 Reactions and rate constants related to the sCI chemistry

Reaction		Rate constant ($cm^3\ s^{-1}$)	References
ETHE + O_3	→ … + 0.37×sCI_1	9.14×10^{-15}	Sarwar et al. (2013)
OLE1 + O_3	→ … + 0.319×sCI_1	2.62×10^{-15}	Sarwar et al. (2013)
OLE2 + O_3	→ … + 0.319×sCI_2	5.02×10^{-16}	Sarwar et al. (2013)
ISOP + O_3	→ … + 0.22×sCI_3	7.88×10^{-15}	Sarwar et al. (2013)
TERP + O_3	→ … + 0.21×sCI_3	1.08×10^{-15}	Sarwar et al. (2013)
$sCI_{1,2,3}$ + SO_2	→ SULF	3.9×10^{-11}	Welz et al. (2012)
$sCI_{1,2,3}$ + NO_2	→ NO_3	7.0×10^{-12}	Welz et al. (2012)
$sCI_{1,2,3}$ + H_2O	→	1.97×10^{-18}	Ying et al. (2014)

Note: SULF represents sulfuric acid.

Atmos. Chem. Phys. Discuss., https://doi.org/10.5194/acp-2019-313
Manuscript under review for journal Atmos. Chem. Phys.
Discussion started: 13 May 2019

Figure Captions

Figure 1 WRF-Chem simulation domain with topography height. The red filled circles show the locations of the cities with ambient air quality monitoring sites, and the size of the circles represents the number of sites in each city. The white and black filled rectangle denotes the weather station and NCNST observation site in Beijing.

Figure 2 Temporal variations of the simulated (blue line) and observed (black dots) near-surface (a) temperature, (b) relative humidity, (c) wind speed, and (d) wind direction at the weather station in Beijing from 04 to 15 July 2015.

Figure 3 Comparison of observed (black dots) and simulated (blue line) diurnal profiles of near surface hourly (a) $PM_{2.5}$, (b) O_3, (c) NO_2, and (d) SO_2 averaged over all ambient monitoring stations in BTH from 04 to 15 July 2015.

Figure 4 Spatial distributions of average (a) $PM_{2.5}$, (b) peak O_3, (c) NO_2, and (d) SO_2 mass concentrations from 04 to 15 July 2015. Colored dots, colored contour, and black arrows are observations and simulations of air pollutants, and simulated surface winds, respectively.

Figure 5 Comparison of observed (black dots) and simulated (blue line) diurnal profiles of hourly submicron (a) nitrate, (b) ammonium, (c) SOA, and (d) POA mass concentrations at NCNST site in Beijing from 04 to 15 July 2015.

Figure 6 (a) Comparison of observed (black dots) and simulated (blue line) diurnal profiles of hourly submicron sulfate mass concentration, and temporal variation of simulated sulfate contribution of the (b) HR_SO_2, (c) OH_SO_2, (d) primary emission, and (e) sCI_SO_2 to the sulfate concentration at NCNST site in Beijing from 04 to 15 July 2015.

Figure 7 Temporal variation of the average simulated pH in Beijing from 04 to 15 July 2015

Figure 8 Spatial distributions of average sulfate contributions of the (a) HR_SO_2, (b) OH_SO_2, (c) primary emission, and (d) sCI_SO_2 in BTH from 04 to 15 July 2015.

Figure 9 Temporal variations of the simulated average sulfate concentration contributed by the sCI_SO_2 (Blue line: B-case; Red line: S1-case; Green line: S2-case) in BTH from 04 to 15 July 2015.

Atmos. Chem. Phys. Discuss., https://doi.org/10.5194/acp-2019-313
Manuscript under review for journal Atmos. Chem. Phys.
Discussion started: 13 May 2019

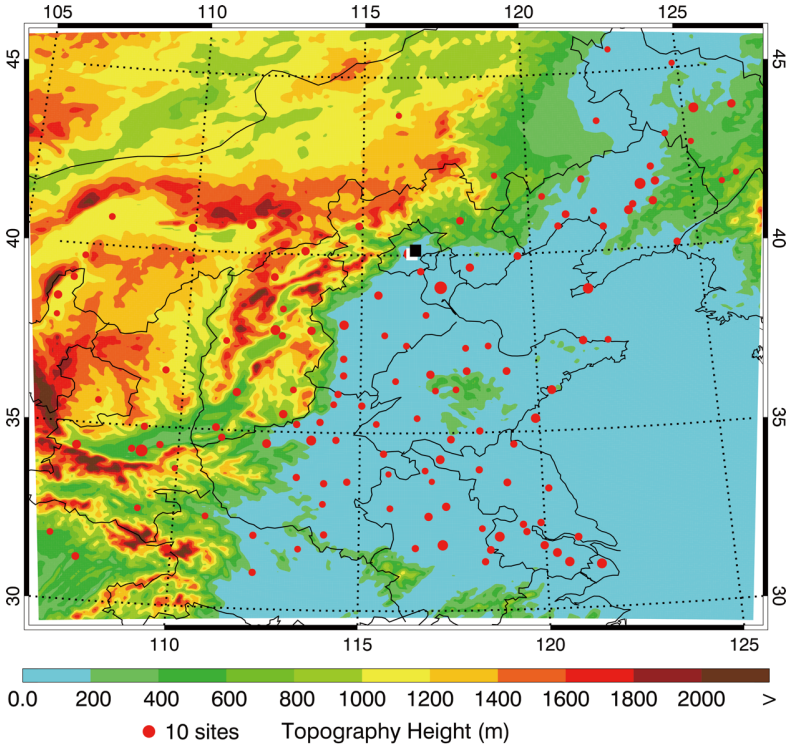

Figure 1 WRF-Chem simulation domain with topography height. The red filled circles show the locations of the cities with ambient air quality monitoring sites, and the size of the circles represents the number of sites in each city. The white and black filled rectangle denotes the weather station and NCNST observation site in Beijing.

Atmos. Chem. Phys. Discuss., https://doi.org/10.5194/acp-2019-313
Manuscript under review for journal Atmos. Chem. Phys.
Discussion started: 13 May 2019

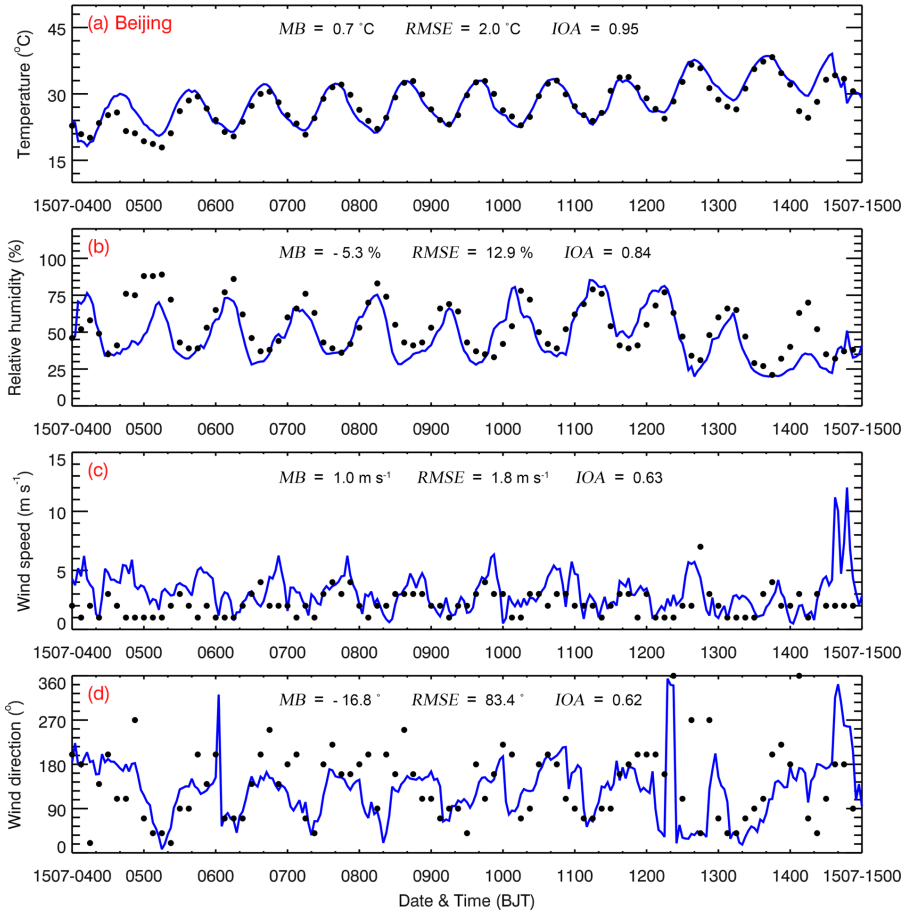

Figure 2 Temporal variations of the simulated (blue line) and observed (black dots) near-surface (a) temperature, (b) relative humidity, (c) wind speed, and (d) wind direction at the weather station in Beijing from 04 to 15 July 2015.

Atmos. Chem. Phys. Discuss., https://doi.org/10.5194/acp-2019-313
Manuscript under review for journal Atmos. Chem. Phys.
Discussion started: 13 May 2019

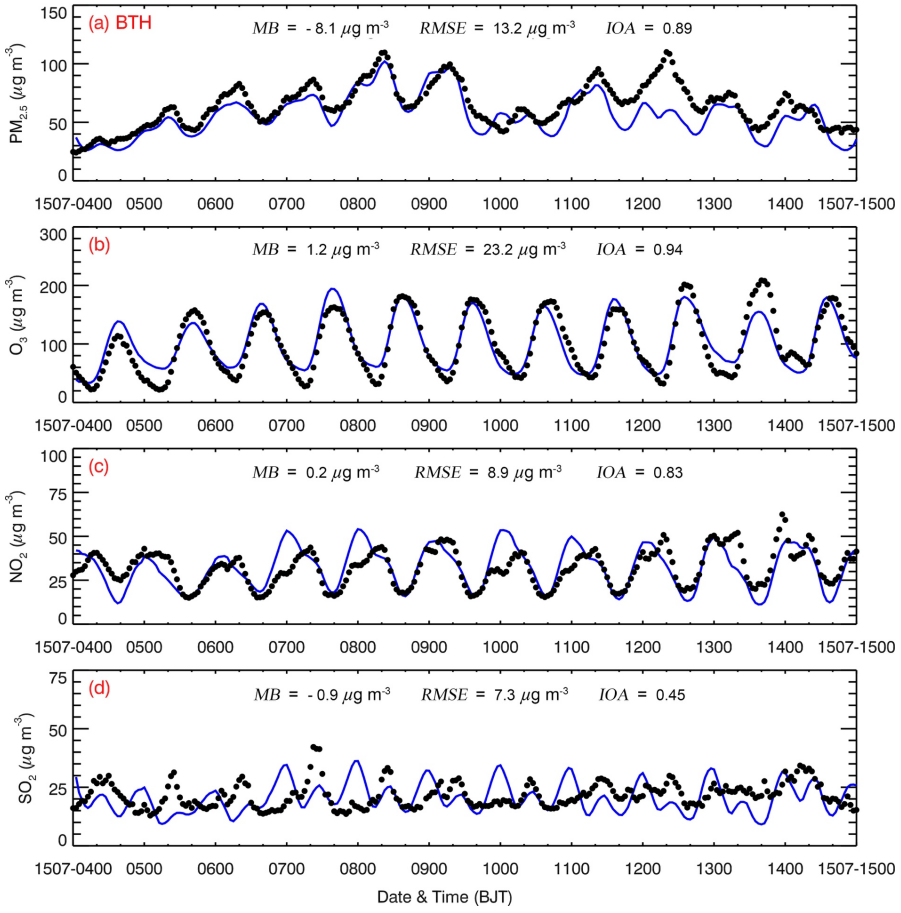

Figure 3 Comparison of observed (black dots) and simulated (blue line) diurnal profiles of near surface hourly (a) $PM_{2.5}$, (b) O_3, (c) NO_2, and (d) SO_2 averaged over all ambient monitoring stations in BTH from 04 to 15 July 2015.

Atmos. Chem. Phys. Discuss., https://doi.org/10.5194/acp-2019-313
Manuscript under review for journal Atmos. Chem. Phys.
Discussion started: 13 May 2019

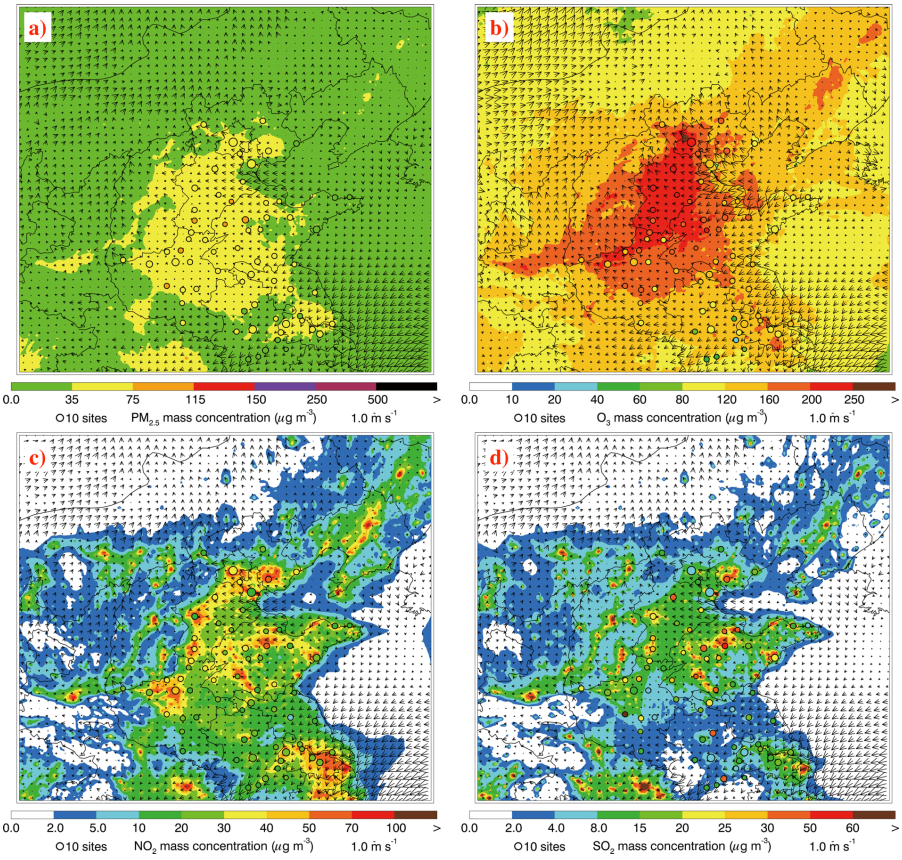

Figure 4 Spatial distributions of average (a) $PM_{2.5}$, (b) peak O_3, (c) NO_2, and (d) SO_2 mass concentrations from 04 to 15 July 2015. Colored dots, colored contour, and black arrows are observations and simulations of air pollutants, and simulated surface winds, respectively.

Atmos. Chem. Phys. Discuss., https://doi.org/10.5194/acp-2019-313
Manuscript under review for journal Atmos. Chem. Phys.
Discussion started: 13 May 2019

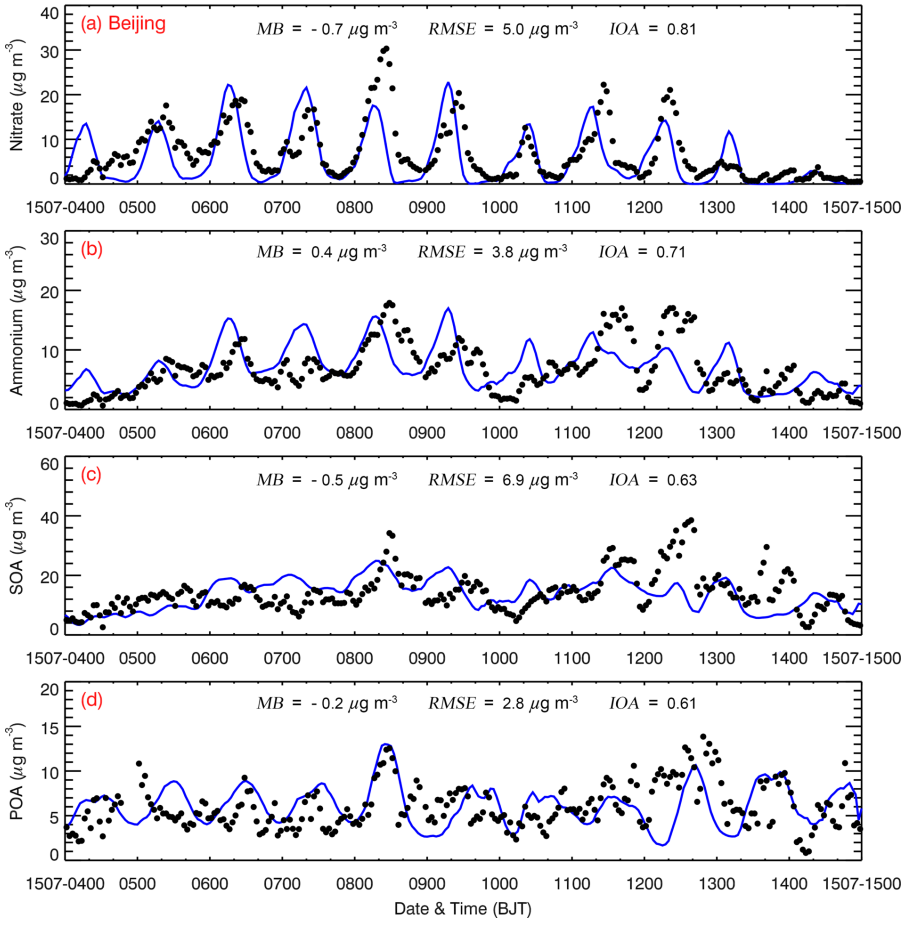

Figure 5 Comparison of observed (black dots) and simulated (blue line) diurnal profiles of hourly submicron (a) nitrate, (b) ammonium, (c) SOA, and (d) POA mass concentrations at NCNST site in Beijing from 04 to 15 July 2015.

Atmos. Chem. Phys. Discuss., https://doi.org/10.5194/acp-2019-313
Manuscript under review for journal Atmos. Chem. Phys.
Discussion started: 13 May 2019

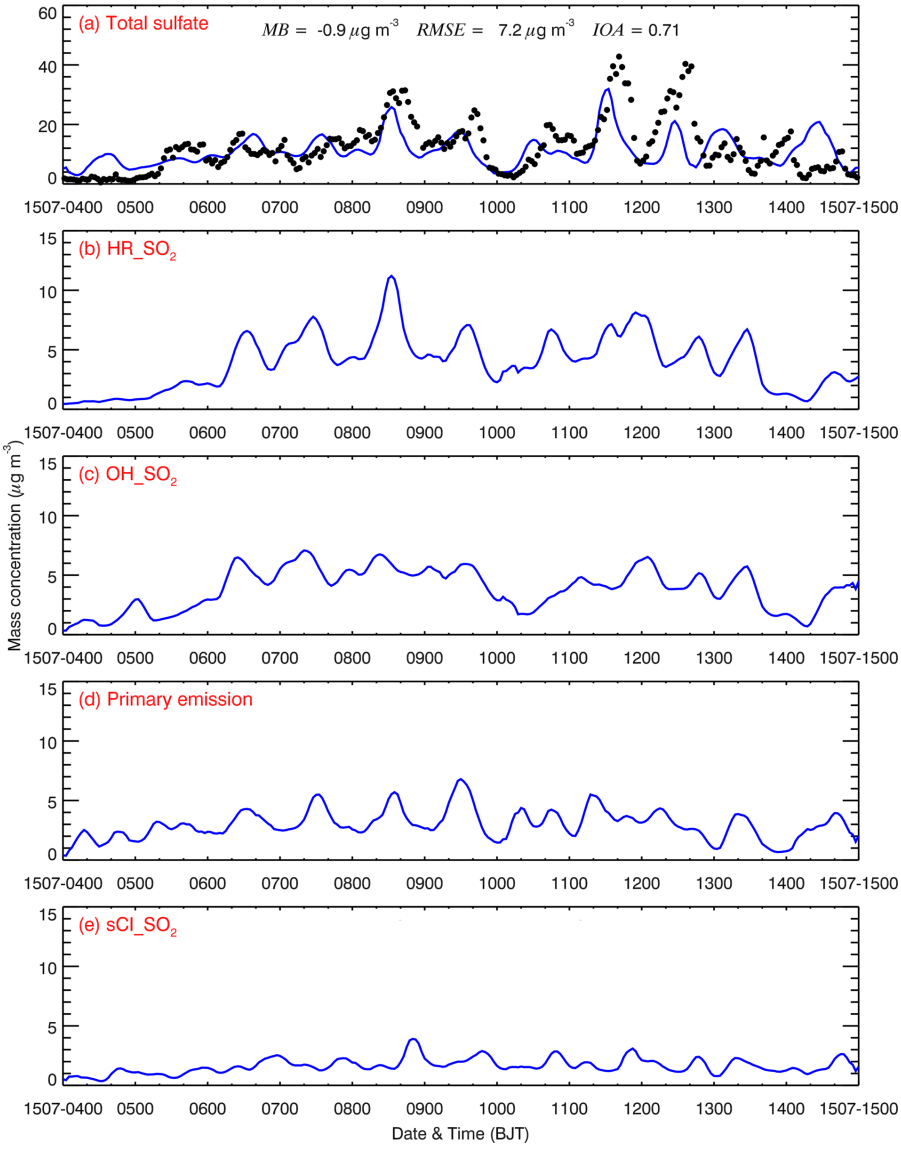

Figure 6 (a) Comparison of observed (black dots) and simulated (blue line) diurnal profiles of hourly submicron sulfate mass concentration, and temporal variation of simulated sulfate contribution of the (b) HR_SO_2, (c) OH_SO_2, (d) primary emission, and (e) sCI_SO_2 to the sulfate concentration at NCNST site in Beijing from 04 to 15 July 2015.

Atmos. Chem. Phys. Discuss., https://doi.org/10.5194/acp-2019-313
Manuscript under review for journal Atmos. Chem. Phys.
Discussion started: 13 May 2019

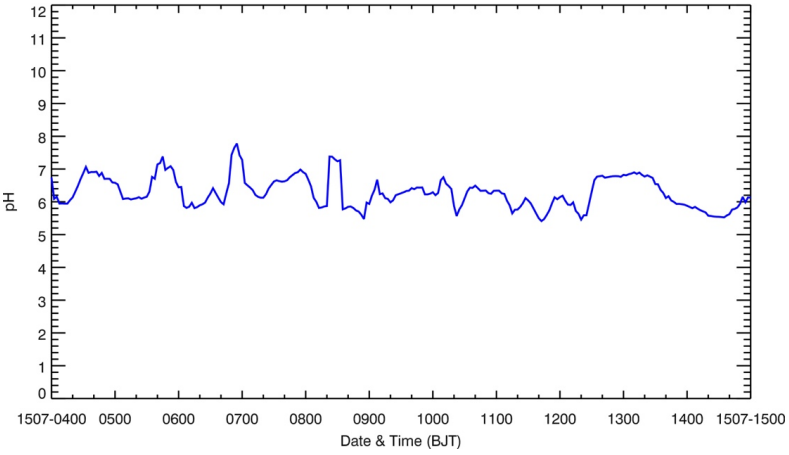

Figure 7 Temporal variation of the average simulated pH in Beijing from 04 to 15 July 2015.

Atmos. Chem. Phys. Discuss., https://doi.org/10.5194/acp-2019-313
Manuscript under review for journal Atmos. Chem. Phys.
Discussion started: 13 May 2019

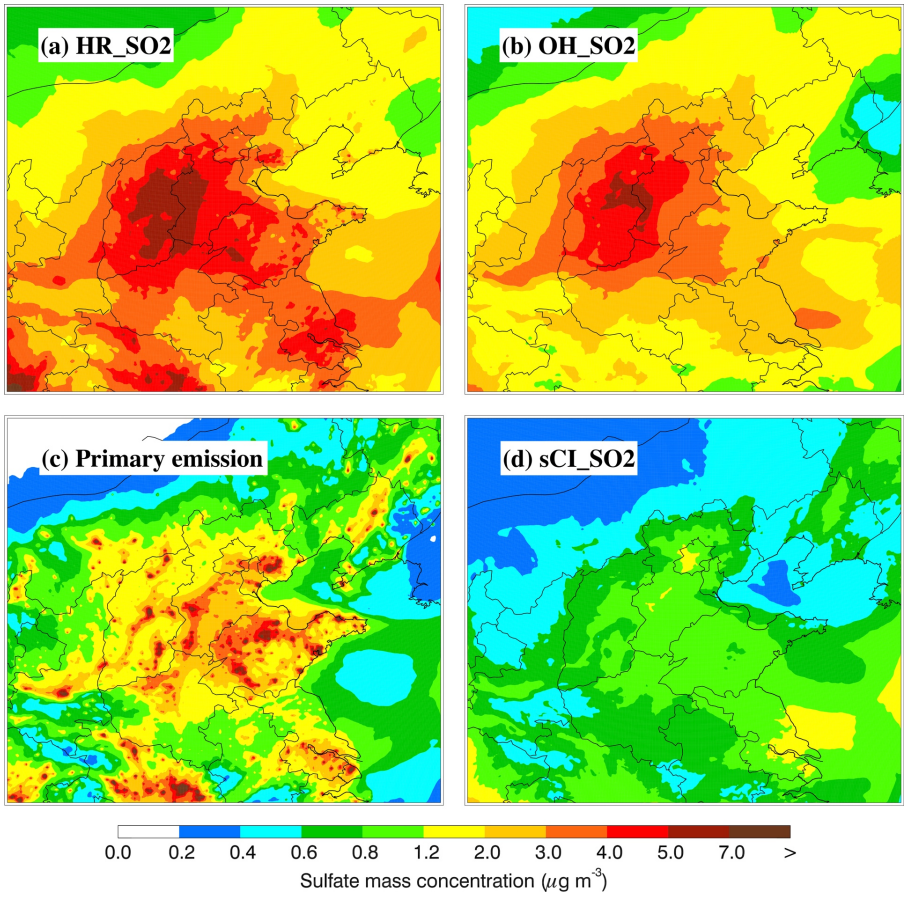

Figure 8 Spatial distributions of average sulfate contributions of the (a) HR_SO_2, (b) OH_SO_2, (c) primary emission, and (d) sCI_SO_2 in BTH from 04 to 15 July 2015.

Atmos. Chem. Phys. Discuss., https://doi.org/10.5194/acp-2019-313
Manuscript under review for journal Atmos. Chem. Phys.
Discussion started: 13 May 2019

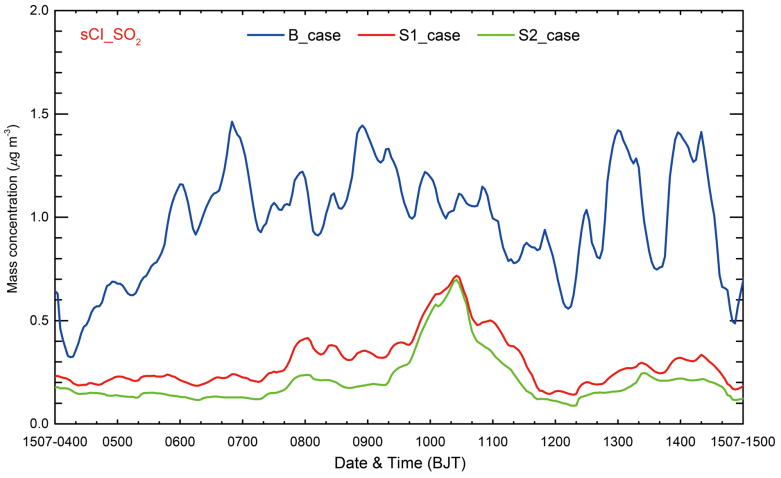

Figure 9 Temporal variations of the simulated average sulfate concentration contributed by the sCl_SO_2 (Blue line: B-case; Red line: S1-case; Green line: S2-case) in BTH from 04 to 15 July 2015.